



An Experimental Investigation of Forces on a Textured Cylinder at Subcritical Reynolds Numbers

H. Karampour^{1†}, Z. Wu¹ and M. S. Mason²

¹ Griffith School of Engineering and Built Environment, Griffith University, Gold Coast Campus, QLD 4222, Australia

² School of Civil Engineering, The University of Queensland, St. Lucia, QLD 4072, Australia

†Corresponding Author Email: h.karampour@griffith.edu.au

(Received December 21, 2020; accepted July 4, 2021)

ABSTRACT

Spanwise deviations from a perfect circular cross-section, affect the aerodynamics and hydrodynamics of cylindrical structures. In this study the ability of a novel wavy cylinder, the textured cylinder, to reduce applied drag and lift forces is investigated experimentally. Three different configurations of the proposed textured geometry, as well as a bare cylinder and a cylinder with helical strakes are 3D printed and tested in an open circuit wind tunnel. Tests are conducted at Reynolds numbers from 3.5×10^4 to 8.0×10^4 . Results show that the time-averaged drag and fluctuating lift forces on the textured cylinder can be 20% and 15% lower than those of a bare cylinder, respectively. Amongst the tested cylinders, the straked cylinder exhibited the lowest fluctuating lift forces. However, the lowest time-averaged drag forces were measured on the textured cylinder, Tex30, through the range of Reynolds numbers tested. The Strouhal number of the Tex30 was found to be between those of the bare and straked cylinders.

Keywords: Textured cylinder; Aerodynamic forces; Strouhal number; Wavy cylinder.

NOMENCLATURE

D	cylinder diameter	ks	surface roughness
F_x	time-averaged streamwise force	p	helical strake pitch length
F_y	the root-mean-square fluctuating lift force in the cross-flow direction	t	wall-thickness
N	number of circumferential triangles	u	streamwise velocity
Re	Reynolds number	α	base angle of a typical triangular facet
R_o	radius of circumscribed cylinder	β	the angle of undulation
S_t	Strouhal number	a_w	the amplitude of surface curve
co	degree of cylinder obliqueness	λ_w	the wavelength of variation
		Δ	the amplitude of undulation

1. INTRODUCTION

The aero- and hydrodynamics of a cylinder are strongly affected by its spanwise irregularities as outlined by Demartino *et al.* (2017). These irregularities can be in the form of spanwise truncation, tapering, tilting, bending, section variation or a combination of these conditions. Most common are cylinders with variable local radii in shape of tapered, discontinuous and wavy geometries. Tapered cylinders and cylinders with discontinuities are common geometries in engineering applications such as heat exchangers,

airport control towers and subsea risers (Demartino *et al.* 2017). Studies by Hsiao and Chiang (1998) and Kappler *et al.* (2005) showed that in uniform subcritical flow, the aerodynamics of a tapered cylinder are similar to that of a uniform cylinder in shear flow. Lim and Lee (2004), and Nakamura *et al.* (2008) investigated the reduction of drag force in discontinuous cylinders at Reynolds numbers (Re) between 3.0×10^3 and 3.8×10^4 . Nakamura *et al.* (2008) and Lim and Lee (2004) showed that the drag forces on discontinuous cylinders can be 15% lower than that on a uniform cylinder of identical diameter. Lam *et al.* (2004) conducted wind-tunnel tests on

wavy cylinders at subcritical Reynold numbers. They found that the root-mean-square fluctuating lift coefficients of the wavy cylinders are much lower than those of a circular cylinder.

Geometry of a wavy cylinder is shown in Fig. 1 (Demartino *et al.* 2017). The wavy geometry is distinguished from a uniform cylinder by two non-dimensional parameters: the normalised amplitude a_w/D_m and the normalised wave-length λ_w/D_m , where a_w is the amplitude of surface curve and λ_w is the wavelength of variation. Lam *et al.* (2004) defined a non-dimensional parameter, co , to express the degrees of cylinder obliqueness.

$$co = \frac{a_w^2}{\lambda_w(D_m - 2a_w)} \quad (1)$$

Lam *et al.* defined the Reynolds number (Re), based on the free-stream velocity and the nominal cylinder diameter (D), and investigated the drag forces in wavy cylinders with $co = 6.94 \times 10^{-3}$, 4.44×10^{-3} and 1.0×10^{-2} , at $2.0 \times 10^4 < Re < 5.0 \times 10^4$. Their study showed 16.3%, 12.5% and 16.2% reduction in the mean drag force for the 3 values of obliqueness, respectively. A 22% reduction in drag force was reported by Nguyen and Jee (2004) for a wavy cylinder with $co = 3.33 \times 10^{-2}$ at $Re = 1.0 \times 10^4$. The reduction in forces on wavy cylinders can be explained by the dynamics of the flow conditions. Ahmed *et al.* (1993) and Lam *et al.* (2004) found that the flow is more stable around the saddle of the wavy cylinder (see Fig. 1). They observed that in contrast to the uniform cylinders, an alternating stream-wise vortex regime is generated along the span of the wavy cylinder with a wave-length equal to D_m . The shear layers at the saddle points spread along the

length of the cylinder and shrink at the nodes. Consequently, the fluctuating pressure and therefore the mean drag and lift are reduced. Another typical type of wavy cylinders are those with continuous helical strakes. These *straked* cylinders are commonly used to mitigate vortex-induced vibrations in Civil Engineering structures (Scruton 1957) and subsea risers (Vandiver 1993; Piran *et al.* 2020). A comprehensive study conducted by Quen *et al.* (2014) on hydrodynamic forces of vibrating straked cylinders showed that the helical strake with pitch length $p = 10D$ and fin height $h = 0.10D$ give the lowest mean drag force. The greatest reduction in fluctuating lift, when compared with a smooth circular cylinder of diameter D , was observed in straked cylinders with fin height of $0.15D$ and pitch length between $5D$ to $15D$ (Quen *et al.* 2014).

This study aims to investigate the aerodynamic forces on a novel wavy cylinder with a textured geometry (Fig. 2). The textured geometry (mimicking the post-buckling pattern of axially compressed thin cylinder) is cylindrical in the global sense with a local texture rather than a smooth wall. Previous studies have shown that the proposed textured geometry has favourable structural (Albermani *et al.* 2011; Karampour and Albermani 2016) characteristics compared with that of conventional cylindrical configurations, which can be exploited in deep subsea applications. A recent numerical study (Karampour *et al.* 2018) showed that at very low Reynolds number ($Re < 200$), the mean drag coefficient of the textured geometry is almost equal to that of the circular cylinder while the root-mean-square fluctuating lift

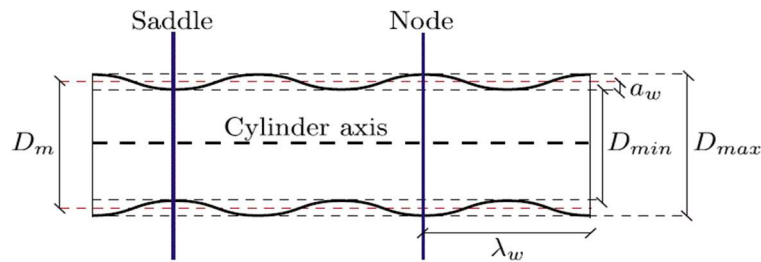


Fig. 1. Geometry and characteristics of a wavy cylinder (Demartino *et al.* 2017).

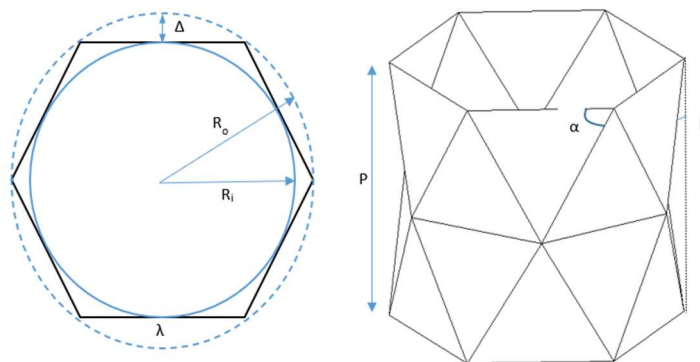


Fig. 2. Textured geometry showing (a) the circumscribed and inscribed circles to the hexagon, and (b) the base angle α and pitch length p .

coefficient of textured geometry is 15% smaller than that of a circular cylinder. In the current study the aerodynamic forces on three textured cylinder with different configurations are investigated experimentally at subcritical Reynolds numbers between $3.5 \times 10^4 < Re < 8.0 \times 10^4$. Tests are also carried out for this Re range on a bare cylinder and a straked cylinder, with mean drag force coefficient, fluctuating lift force and Strouhal number compared with those measured on the textured cylinders.

2. THE TEXTURED GEOMETRY

As shown in Fig. 2, the basic building block of the textured cylinder is the isosceles triangular facet. The geometry of the textured cylinder can be described in terms of four basic parameters. These are; the radius of the equivalent circumscribed cylinder, R_o , the wall-thickness, t , the number of circumferential triangles, N , and the base angle of a typical triangular facet, α . For the textured cylinder shown in Fig. 2, $N=6$ and the remaining geometric variables shown in the figure are functions of R_o , N and α as given in the following relations

$$\theta = \frac{\pi}{2} - \frac{\pi}{N} \quad \lambda = 2R_o \sin \frac{\pi}{N} \quad \Delta = R_o \left(1 - \cos \frac{\pi}{N} \right)$$

$$p = R_o \sin \frac{\pi}{N} \tan \alpha$$

$$\beta = \sin^{-1} \left[\frac{\left(1 - \cos \frac{\pi}{N} \right)}{\sin \frac{\pi}{N} \tan \alpha} \right] \quad (2)$$

where α is the base angle of a circumferential triangle, Δ is the amplitude of undulation, β is the angle of undulation (inclination of the triangular facet relative to the cylindrical axis), p and λ are the pitch and base length, respectively, of a typical triangular facet. For a given N (and hence Δ), an increase in the base angle α results in a reduction in the angle of undulation β . Further, N has a paramount effect on the textured form both in the circumferential and longitudinal directions.

3. SPECIMENS AND TEST SET-UP

A segment of all tested specimens are shown in Fig. 3a. From left to right these are: (1) straked cylinder with helical strakes of pitch length $p=6D_i$ and fin height $h=0.1D_i$, (2) bare cylinder with diameter $D_i=50\text{mm}$, (3) Tex60, a textured cylinder with base angle $\alpha=60^\circ$, (4) Tex45, textured cylinder with base angle $\alpha=45^\circ$, and (5) Tex30 a textured cylinder with base angle $\alpha=30^\circ$. The three textured cylinders all had $N=6$ circumferential triangles, inner radii of $R_i = 25$ mm and outer radii of $R_o = 28\text{mm}$. All specimens were 3D printed using high-strength nylon. The degree of obliqueness, co (Eq. 1) of the textured cylinder can be defined by two non-dimensional parameters: the normalised amplitude, Δ/D_o , and the normalised wave-length, p/D_o , (see

Fig. 2). These values are represented for different textured configurations in Table 1.

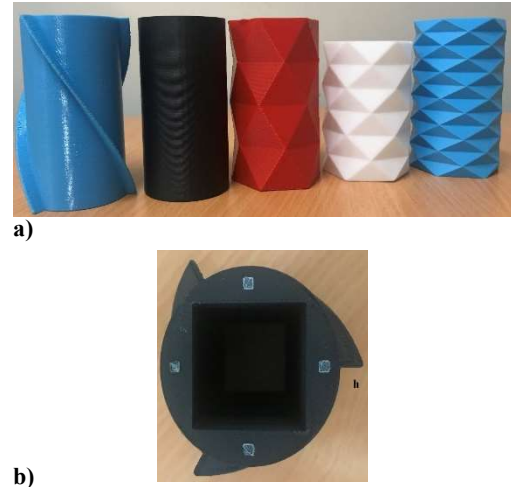


Fig. 3. (a) Specimens from left to right: straked, bare, Tex60, Tex45 and Tex30, and (b) the cross-section of the straked cylinder showing the orientation and fin height (h) of the strake.

The specimens were tested in an open circuit wind tunnel at The University of Queensland (Yang and Mason 2019). The test section of the wind tunnel is shown in Fig. 4a and is 762×762 mm in cross section and approximately 2.4 m long. Each specimen is positioned in the centre of the tunnel 1.5 m downstream from the test section inlet. Prior to the inlet, flow passes through a honeycomb and two turbulence reduction screens then through a 6:1 contraction. Freestream turbulence in the tunnel is $\sigma_u/u < 0.01$, where σ_u is the standard deviation of streamwise velocity, u . Mean u and σ_u over the length of test specimen varied by less than 0.2%, and was therefore considered uniform. A rigid spine was inserted inside the hollow specimens and mounted on top of an ATI Mini85 load cell (shown in Fig. 4b) so global forces on the body could be measured. The load cell is a 6-component balance that measures drag and lift forces through the range 0 – 475 N with a measurement accuracy of less than 1.5%. Similarly, it measures torque around its three primary axes to a maximum value of 20 Nm and an accuracy of 1.25%.

Table 1 Non-dimensional obliqueness parameters of the textured cylinders

	Δ/D_o	p/D_o	co
Tex60	0.067	1.000	0.012
Tex45	0.067	0.578	0.021
Tex30	0.067	0.334	0.036

The central spine was initially made of an aluminium rectangular hollow section (RHS). However, due to

excessive vibrations, this was replaced with a steel RHS. The spine was welded onto a plate and the assembly was bolted to the load cell at 8 Nm torque by using a torque wrench. The load cell was secured onto a heavy rack and isolated from the wind tunnel. As shown in Fig. 4a, 300mm diameter end plates were used on the top and bottom of the test section to reduce any wall effects and promote two-dimensional flow. Plastic tube was positioned around the spine below the bottom end plate so no wind loads were applied to this section. A 2mm gap was maintained between the specimen and the end plates (both top and bottom) to ensure no contact and subsequent transfer of forces between the two. The clear length of the 3D printed specimen between the endplates (Fig. 3a) was equal to $L=600\text{mm}$ to maintain an aspect ratio ($\lambda=L/D_i$) of 12 in all cylinders. According to [Zdravkovich et al. \(1998\)](#) at aspect ratio greater than 10, the cylinder can be considered long and the assumption of two-dimensional flow is reasonable.

To measure the test velocity (u), a Pitot tube was placed between the cylinder and the side wall, at mid height of the cylinder and connected to a u-tube manometer. LabView was used to monitor, control and record the wind tunnel and forces measured by the load cell.



Fig. 4. (top) The straked specimen inside the test section of the wind tunnel, and (bottom) the spine-load cell connection.

4. RESULTS AND DISCUSSION

The aerodynamic force coefficients for the tested specimens are calculated using

$$C_D = \frac{2F_x}{\rho_{air}u^2A}, \quad C_L = \frac{2F'_y}{\rho_{air}u^2A} \quad (3)$$

where u is the measured mean wind velocity. F_x is the time-averaged streamwise force, and F'_y is the root-mean-square fluctuating lift force in the cross-flow direction. To ensure aerodynamic force coefficients calculated using Eq. 3 provide a meaningful comparison between forces applied to each cylinders, the frontal area (A) of all specimens were taken to be equal. That is, the area (A) was calculated by multiplying the length of the sample ($L=600\text{ mm}$) by the diameter of the inscribed circle (bare cylinder) equal to 50mm. Density of air was taken as $\rho_{air}=1.17\text{kg/m}^3$. The Reynolds number ($Re=uDi/\nu$) was calculated based on kinematic viscosity $\nu=1.81\times 10^{-5}$ (kg/m.s). The measured mean drag coefficients for the bare cylinder are compared to reported ([Achenbach and Heinecke 1981](#)) drag coefficients of smooth and rough cylinders in Fig. 5. The normalised surface roughness of the bare cylinder used in the current tests was measured as $k_s/D_i=4.6\times 10^{-3}$. As expected, the current drag results of the bare cylinder with $k_s/D_i=4.6\times 10^{-3}$ are slightly higher than those of the cylinder with $k_s/D_i=1.9\times 10^{-3}$ ([Achenbach and Heinecke 1981](#)).

Time-averaged drag, C_D , and root-mean-square fluctuating lift coefficients, C_L , of the tested cylinders are plotted in Fig. 6. The maximum C_D is observed for the textured sample with base angle $\alpha=60^\circ$, with the minimum measured for the textured sample with $\alpha=30^\circ$. Concerning the degrees of obliqueness, co (Eq. 1) of the textured cylinders represented in Table 1, it can be inferred that by increasing co and decreasing the wavelength p , the drag force of the textured cylinder will decrease. [Lam et al. \(2004\)](#) investigated the effect of degree of obliqueness on the reduction of drag coefficient in wavy cylinders, using wind-tunnel tests. Lam et al. found that with Re ranging from 2.0×10^4 to 5.0×10^4 (similar to the current study), a drag reduction of up to 20% can be achieved if co is increased by 2.26 times. For current tests, the co of Tex30 is 3 times that of Tex60. The current results in Fig. 6 suggest that drag of Tex30 is on average 18% lower than Tex60. The measured drag of the cylinder with helical strakes is lower than the bare cylinder in the current study. This agrees with previously published results of [Quen et al. \(2014\)](#) who reported lower drag forces in straked cylinders compared to bare cylinders.

The fluctuating lift coefficients for each cylinder is shown in Fig. 6. The lowest lift corresponds to the straked cylinder. However, all of the textured cylinders had cross-flow coefficients lower than the bare cylinder. Amongst the textured cylinders, Tex60 shows the largest lift coefficients and Tex30 has the lowest C_L . Similar to the drag coefficients,

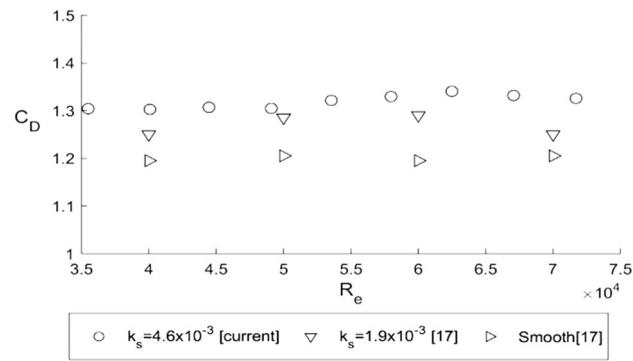


Fig. 5. Comparison between drag coefficients (C_D) of the current bare cylinder with normalised surface roughness $k_s/D_i=4.6 \times 10^{-3}$ and those reported by Achenbach and Heinecke (1981) for smooth cylinder and cylinder with $k_s/D_i=1.9 \times 10^{-3}$.

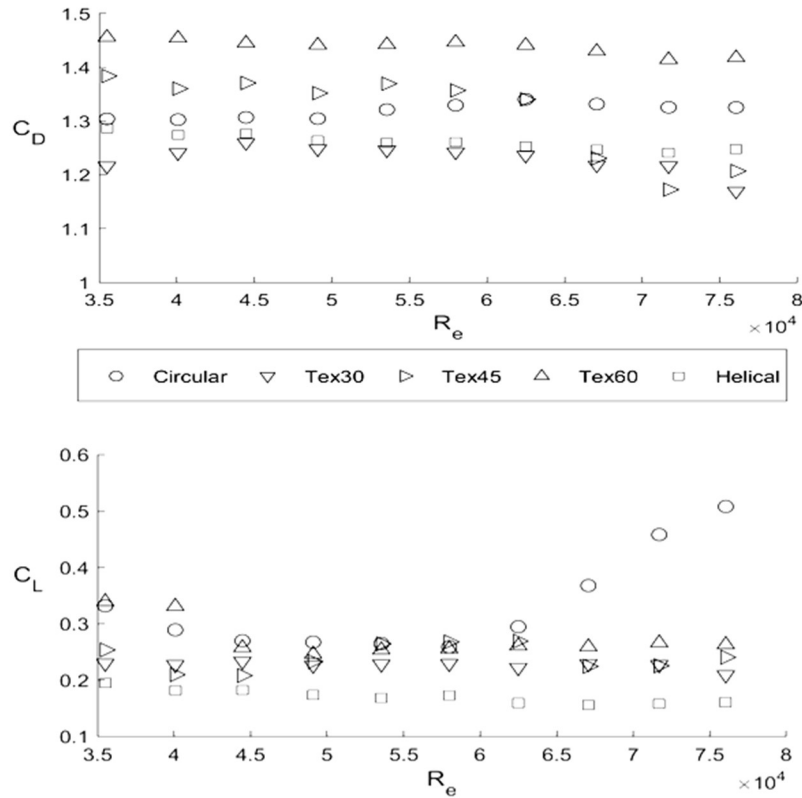


Fig. 6. Drag (C_D) and lift (C_L) coefficients of the tested cylinders.

by increasing the obliqueness degree (α), the cross-flow coefficients of the textured geometry drop. The lift coefficient of the Tex30 is on average 15% lower than Tex60.

The power spectra of the fluctuating lift forces measured on the circular, helical and Tex30 cylinders at $Re=6.7 \times 10^4$ are plotted in Fig. 7. For sake of comparison the textured cylinder with the lowest C_L (Tex30) is selected. The peak vortex-shedding frequencies f_s are presented in Table 2 normalised by mean velocity u and diameter D , using

the Strouhal number (Eq. 4) and are represented in Table 2.

$$St = \frac{f_s D}{u} \quad (4)$$

It can be seen from Fig. 7 that for the bare cylinder (Circular) and Tex30, the peaks of the spectra are sharp and occur at fixed frequencies. This said, the peak is considerably narrower for Tex30 than the bare cylinder. The Strouhal number St of 0.195 found herein for the bare cylinder is consistent with values reported

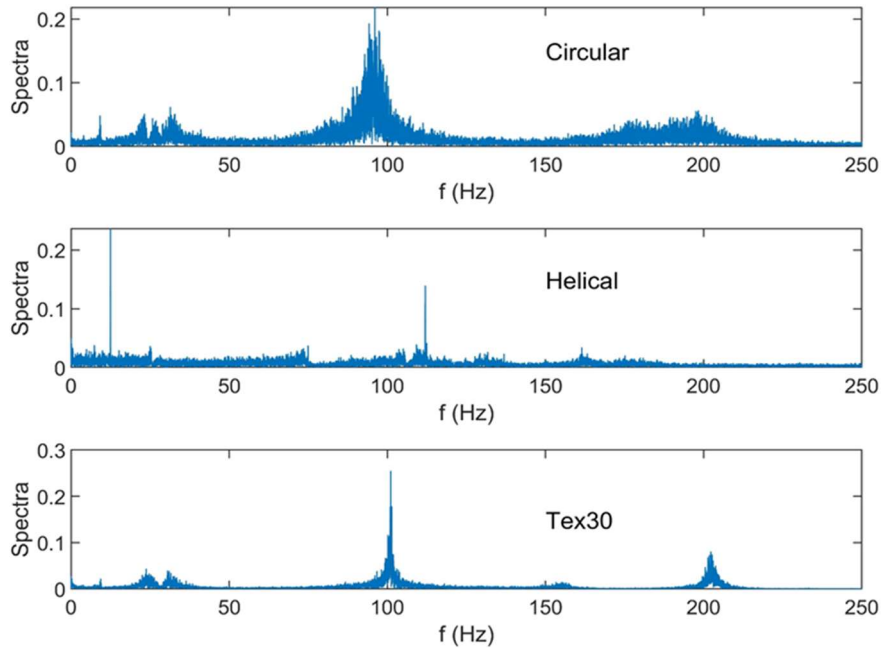


Fig. 7. Power spectra vs. frequency for fluctuating lift force of the cylinders at $Re=6.7 \times 10^4$, (a) Circular, (b) Helical, and (c) Tex30.

previously (Zhou *et al.* 2011; Xue *et al.* 2015; Qiu *et al.* 2017). The variation observed in the frequencies of the cylinder with helical strakes in Fig. 7, can be related to the spanwise motion of the fluid in the downstream of the straked cylinder. This effect has been previously observed in both computational fluid dynamics (CFD) (Constantinides *et al.* 2006) and wind tunnel (Zhou *et al.* 2011) studies. The Strouhal number of the Tex30 is in between those of the bare and straked cylinders, and is consistent with the lift coefficient trend shown in Fig. 6 at $Re=6.7 \times 10^4$.

Table 2 Vortex-shedding frequencies and Strouhal numbers

	f_s (Hz)	St
Circular	96.0	0.195
Helical	112.0	0.227
Tex30	101.1	0.205

4. CONCLUSION

An experimental investigation of the in line and cross-flow forces applied to textured cylinders was conducted. The tests were carried out on cylinders with diameter of 50mm and length of 600mm in an open circuit wind-tunnel. Results showed that in the subcritical range ($3.5 \times 10^4 < Re < 8.0 \times 10^4$), all textured configurations experienced cross-flow force coefficients smaller than on a bare cylinder with equivalent diameter. The textured cylinder with base angle of $\alpha=30^\circ$ (Tex30) experienced the lowest drag and lift coefficients compared to other textured configurations. It is understood that the drag

reduction of the textured geometry is directly related to its degree of obliqueness (co). Similar to previously published results of wavy cylinders (Lam *et al.* 2004), by tripling the obliqueness degree, co , the drag coefficient of the textured cylinders reduced by almost 20%. Lift coefficients reduced by 15% for the same increase in co . A 5% increase in the vortex-shedding frequency of the Tex30 compared to the bare cylinder was calculated from the analysis of the energy spectra. Current results suggest that the textured geometry has benefits in reducing the in line and cross-flow forces and therefore may be a potential solution for passive suppression of the vortex-induced vibration in slender cylinders, such as subsea risers.

REFERENCES

- Achenbach, E. and E. Heinecke (1981). On vortex shedding from smooth and rough cylinders in the range of Reynolds numbers 6×10^3 to 5×10^6 . *Journal of Fluid Mechanics* 109, 239-251.
- Ahmed, A., M. J. Khan and B. Bays-Muchmore (1993). Experimental investigation of a three-dimensional bluff-body wake. *AIAA Journal* 31(3), 559-563.
- Albermani, F., H. Khalilpasha and H. Karampour (2011). Propagation buckling in deep sub-sea pipelines. *Engineering Structures* 33(9), 2547-2553.
- Constantinides, Y. and O. H. Oakley Jr (2006, January). Numerical prediction of bare and straked cylinder VIV. In *International Conference on Offshore Mechanics and Arctic Engineering* (Vol. 47497, pp. 745-753).

- Demartino, C. and F. Ricciardelli (2017). Aerodynamics of nominally circular cylinders: A review of experimental results for Civil Engineering applications. *Engineering Structures* 137, 76-114.
- Hsiao, F. B. and C. H. Chiang (1998). Experimental study of cellular shedding vortices behind a tapered circular cylinder. *Experimental Thermal and Fluid Science* 17(3), 179-188.
- Kappler, M., W. Rodi, S. Szepessy and O. Badran (2005). Experiments on the flow past long circular cylinders in a shear flow. *Experiments in Fluids* 38(3), 269-284.
- Karampour, H. and F. Albermani (2016). Buckle interaction in textured deep subsea pipelines. *Ships and Offshore Structures* 11(6), 625-635.
- Karampour, H., Z. Wu, J. Lefebure, D. S. Jeng, A. Etemad-Shahidi and B. Simpson (2018). Modelling of flow around hexagonal and textured cylinders. *Proceedings of the Institution of Civil Engineers-Engineering and Computational Mechanics* 171(3), 99-114.
- Lim, H. C. and S. J. Lee (2004). Flow control of a circular cylinder with O-rings. *Fluid Dynamics Research* 35(2), 107.
- Nakamura, H. and T. Igarashi (2008). Omnidirectional reductions in drag and fluctuating forces for a circular cylinder by attaching rings. *Journal of wind engineering and industrial aerodynamics* 96(6-7), 887-899.
- Nguyen, A. T. and S. Jee (2004, May). Experimental investigation on wake behind a sinusoidal cylinder. In *Proceedings of the Proceeding of Tenth Asian Congress of Fluid Mechanics*.
- Piran, F., H. Karampour and P. Woodfield (2020). Numerical Simulation of Cross-Flow Vortex-Induced Vibration of Hexagonal Cylinders with Face and Corner Orientations at Low Reynolds Number. *Journal of Marine Science and Engineering* 8(6), 387.
- Qiu, W., D. Y. Lee, H. Lie, J. M. Rousset, T. Mikami, S. Sphaier, L. Tao, X. Wang and V. Magarovskii (2017). Numerical benchmark studies on drag and lift coefficients of a marine riser at high Reynolds numbers. *Applied Ocean Research* 69, 245-251.
- Quen, L. K., A. Abu, N. Kato, P. Muhamad, A. Sahekhaini, and H. Abdullah (2014). Investigation on the effectiveness of helical strakes in suppressing VIV of flexible riser. *Applied Ocean Research* 44, 82-91.
- Scruton, C. (1957). A means for avoiding wind-excited oscillations of structures with circular or nearly circular cross section. *National Physical Laboratory (UK), Aero Rep.*
- Vandiver, J. K. (1993). Dimensionless parameters important to the prediction of vortex-induced vibration of long, flexible cylinders in ocean currents. *Journal of Fluids and Structures* 7(5), 423-455.
- Xue, H., K. Wang and W. Tang (2015). A practical approach to predicting cross-flow and in-line VIV response for deepwater risers. *Applied ocean research* 52, 92-101.
- Yang, T. and M. S. Mason (2019). Aerodynamic characteristics of rectangular cylinders in steady and accelerating wind flow. *Journal of Fluids and Structures* 90, 246-262.
- Zdravkovich, M. M., A. J. Flaherty, M. G. Pahle and I. A. Skelthorne (1998). Some aerodynamic aspects of coin-like cylinders. *Journal of Fluid Mechanics* 360, 73-84.
- Zhou, T., S. M. Razali, Z. Hao and L. Cheng (2011). On the study of vortex-induced vibration of a cylinder with helical strakes. *Journal of Fluids and Structures* 27(7), 903-917.